JPE 9-4-12

Filter Design for Grid-Connected Single-Phase Inverters

Hyosung Kim†

†School of EE and Control Engineering, Kongju National University, Korea

ABSTRACT

This paper proposes a filter design guideline for grid-connected single-phase inverters. By analyzing the instantaneous voltage applied to the filter inductor, the switching ripple current through the filter inductor can be precisely calculated. Therefore, filter inductance can be designed accurately, which guaranties that the switching ripple current will be under the target value. The proposed filter design method is verified by experiment.

Keywords: Grid-connected Inverters, Single-phase PWM inverters, Switching ripple current, Filter design

1. Introduction

Distributed power generation systems (DPGS) are widely exploited alongside the development of renewable energy systems [1, 2]. DPGSs cover wide power ranges from 1kW class residential applications to several hundred MW class generation parks. Medium and small scale DPGSs are normally connected to grid systems through utility interactive inverters that inject grid current by means of current mode control operation [3-7].

Since the power quality of the grid interface is influenced by the quality of the injection current, the current quality is generally regulated by utility companies [8, 9]. For example, the total demand distortion (TDD) of a 10-minute averaged value for the injection current on a DPGS should not exceed 5%, and the even harmonics should be held under 25% to the neighbored harmonic limitation.

Manuscript received May 26, 2009; revised June 13, 2009
†Corresponding Author: hyoskim@kongju.ac.kr
Tel: +82-41-521-9167 ; Fax:+82-41-532-2671, Kongju Nat'l Univ.
School of EE and Control Engineering, Kongju Nat'l Univ., Korea

$$TDD = \frac{\sqrt{\sum_{h=2}^{40} I^2(h)}}{I_{rate}} \times 100\ [\%] \tag{1}$$

Moreover, there exist higher order harmonics based on the switching frequency of the utility inverters which come from the circuit condition between the pulse-width modulation (PWM) switching pattern and the grid voltages. Thus, to evaluate the influence of utility inverters on the power quality of a grid interface, both the low order harmonics described by (1), and the high order harmonics described by (2) should be considered [10, 11].

$$I_{rms,sw} = \frac{\sqrt{\sum_{h=41}^{400} I^2(h)}}{I_{rate}} \times 100\ [\%] \tag{2}$$

The current ripples resulting from the high frequency switching of the utility inverters can be attenuated not by controllers, but by passive filters [12-17]. The influence of the ripple current on power quality can be evaluated by the ripple factor (RF) defined by (3).

$$RF_{sw} = \frac{I(h_{sw})}{I_{rate}} \times 100\ [\%] \quad (3)$$

This paper analyzes the relation between the filter inductance and the ripple factor according to the PWM pattern of grid-connected single-phase inverters. Based on the analysis, this paper proposes a design guideline to determine accurate filter inductance that satisfies given ripple factor limitation for the grid injection current.

The proposed design guideline not only assures accurate filter inductance in the *L*-filter configuration, but also precisely estimates the ripple factor for the inverter side *L*-filter of the *LCL*-filter configuration, which is necessary to determine exact *LCL*-filter parameters [11]. The proposed design guideline also gives the correct RMS value of the ripple current, which can also be used for the loss calculation of grid-connected inverter systems.

An experiment was performed to test the validity of the proposed theory and design guidelines.

2. Analysis on Ripple Current

2.1 Inverter topology

Fig. 1 describes a single-phase grid-connected inverter using full-bridge topology. If the b-leg switch is not used and the node v_n is directly connected to the DC split O, then the power circuit changes to a half-bridge topology.

The grid voltage e_a is assumed as an ideal sinusoid. To simplify the analysis, the fundamental component of the grid current in Fig. 1 is assumed to be zero. Thus, the fundamental component of the voltage applied on the filter inductor is also zero, as (4):

$$v_{L1} = v_{O1} - e_a = 0 \quad (4)$$

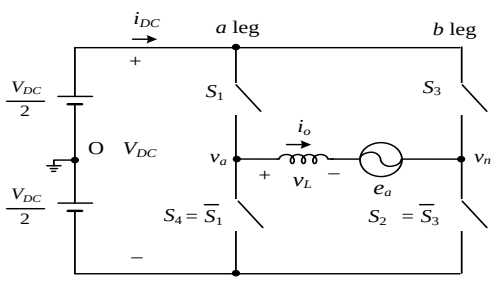

Fig. 1. Topology of a single-phase full-bridge inverter.

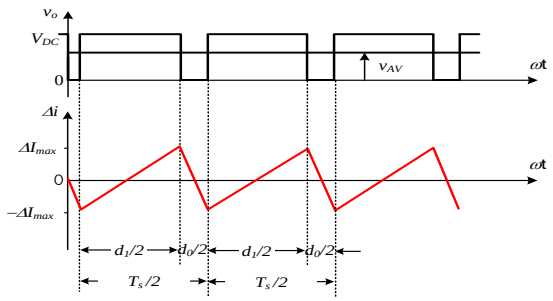

Fig. 2. Output voltage and current waveform of typical single-phase full-bridge inverters.

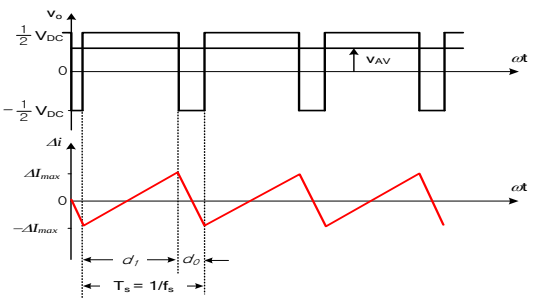

Fig. 3. Output voltage and current waveform of typical single-phase half-bridge inverters.

As can be seen in Fig. 2, single-phase full-bridge inverters normally use unipolar PWM, so that the inverter output voltage v_0 has three step values: V_{dc}, 0 and $-V_{dc}$.

However, single-phase half-bridge inverters have to use bipolar PWM, as shown in Fig. 3, so the inverter output voltage v_0 has two step values: $+V_{dc}/2$ and $-V_{dc}/2$.

Thus, the characteristics of the ripple current are different for the two inverter topologies. This paper analyzes the switching ripple current on the filter inductor according to the two topologies.

2.2 Analysis of ripple current

When the switching frequency f_{sw} is much higher than the utility frequency f_0, the time average value of the inverter output voltage v_{AV} can be regarded as constant during the switching period T_s.

Thus, the filter inductor current of grid-connected single-phase full-bridge inverters during any switching period typically has a waveform as shown by the lower curve in Fig. 2. In this case, the peak-to-peak value of the filter inductor current Δi_{pp} that results from the unipolar

PWM switching can be calculated using (5).

$$\Delta i_{pp} = 2\Delta i_{\max} = \frac{(V_{dc} - v_{AV})}{L}\frac{d_1}{2}T_s \tag{5}$$

Moreover, when the condition described by (4) is applied to single-phase full-bridge inverters during the interval of $0 < \omega t < \pi$, Equations (6) and (7) can be deduced.

$$v_{AV}(\omega t) = d_1(\omega t)V_{dc}, \quad e_a(\omega t) = m_a V_{dc}\sin(\omega t) \tag{6}$$

$$d_1(\omega t) = m_a \sin(\omega t) \tag{7}$$

From (6) and (7), the peak-to-peak value of the filter inductor current during $0 < \omega t < \pi$ can be calculated by (8).

$$\Delta i_{pp}(\omega t) = \frac{V_{dc}T_s}{2L}(1 - m_a \sin(\omega t)) \cdot m_a \sin(\omega t) \tag{8}$$

where, $0 < \omega t < \pi$.

Fig. 4 shows the magnitude distribution of Δi_{pp} of grid-connected single-phase full-bridge inverters according to the parameter of modulation index m_a when the angle is $0 < \omega t < \pi$. $\Delta i_{pp}(\theta)$ has minimum or maximum value when the utility angle θ is: $Sin^{-1}(1/2m_a)$, $\pi/2$ and π-$Sin^{-1}(1/2m_a)$.

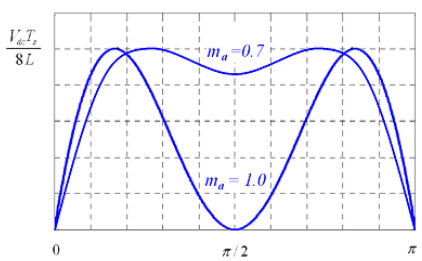

Fig. 4. Magnitude distribution of Δi_{pp} of single-phase full-bridge inverters.

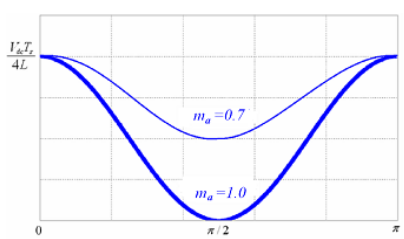

Fig. 5. Magnitude distribution of Δi_{pp} of single-phase half-bridge inverters.

In the same way, the peak-to-peak value of the filter inductor current Δi_{pp} that results from the bipolar PWM switching can be calculated as in (9).

$$\Delta i_{pp}(\omega t) = \frac{V_{dc}T_s}{4L}\{1 - m_a^2 \cdot \sin^2(\omega t)\} \tag{9}$$

here, $0 < \omega t < \pi$.

Fig. 5 shows the magnitude distribution of Δi_{pp} of grid-connected single-phase half-bridge inverters according to the parameter of modulation index m_a when the angle is $0 < \omega t < \pi$. $\Delta i_{pp}(\theta)$ has minimum or maximum value when the utility angle θ is: 0, $\pi/2$ and π.

Since the voltage and current waveforms have half-cycle symmetry, the situation when $\pi < \omega t < 2\pi$ is the same as that when $0 < \omega t < \pi$.

2.3 RMS value of ripple current

The ripple current of utility-interactive single-phase full-bridge inverters consists of triangle waves bounded by $\pm\Delta i_{pp}/2$, as described by Fig.6.

Since RMS value is related with only absolute value, the negative part of the ripple current can be equivalently folded to the positive part in RMS calculation. Thus, the RMS value of Fig.6 can be calculated in the same manner as the RMS value as Fig.7.

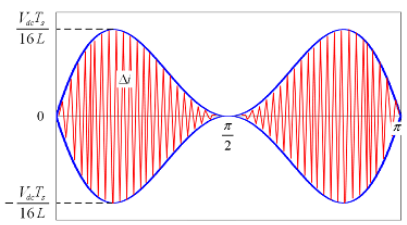

Fig. 6. Typical waveform of the filter inductor ripple current Δi of single-phase full-bridge inverters when m_a=1.0.

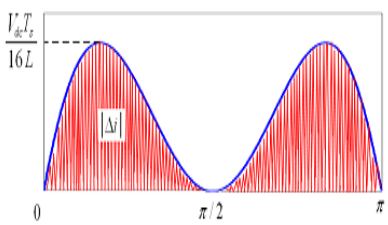

Fig. 7. Equivalent waveform of the ripple current for RMS value.

When the switching frequency f_{sw} is assumed to be an integer multiple of the utility frequency, i.e. $f_{sw}=nf_0$, the number of triangle waves during the 1/4 period (T/4) of the utility angle will be n. Fig. 8 describes the distribution of triangle waves, where the magnitude of any k-th triangle wave can be calculated as in (10).

$$\Delta i_{\max}(\theta_k)=\frac{V_{dc}T_s}{4L}\left[1-m_{a\sin}(\theta_k)\right]\cdot m_a\sin(\theta_k) \tag{10}$$

here, $\theta_k=\frac{(2k-1)\pi}{4n}$, k=1,2, ..., n.

Since the RMS value of each triangle wave is $\Delta i_{\max}(\theta_k)/\sqrt{3}$, as shown by Fig. 8, the RMS value of the ripple current I_r can be calculated as in (11).

$$I_r=\sqrt{\frac{2}{\pi}\sum_{k=1}^{n}\theta_s I_r(k)^2}=\sqrt{\frac{2}{\pi}\sum_{k=1}^{n}\theta_s\frac{\Delta i_{\max}(\theta)^2}{3}} \tag{11}$$

When the switching frequency goes very high, such that θ_s becomes infinitely small, Equation (11) can be written in integral form, as in (12).

$$I_r=\sqrt{\frac{2}{3\pi}\int_0^{\pi/2}\Delta i_{\max}^2(\theta)d\theta} \tag{12}$$

Substituting (8) into (12), Equation (13) can be deduced.

$$I_r=\frac{V_{dc}T_s}{4L}\sqrt{\frac{2}{3\pi}\int_0^{\pi/2}(1-m_a\sin\theta)^2\cdot m_a^2\sin^2\theta d\theta} \tag{13}$$

By calculating the integral in (13), the RMS value of the switching ripple current in single-phase full-bridge inverters can be obtained by (14).

$$\begin{aligned}I_r&=\frac{V_{dc}T_s}{4L}\sqrt{\frac{2}{3\pi}\int_0^{\pi/2}(1-2m_a\sin\theta+m_a^2\sin^2\theta)\frac{m_a^2}{2}(1-\cos 2\theta)d\theta}\\&=\frac{V_{dc}T_s}{4L}\sqrt{\frac{m_a^4}{8}-\frac{8m_a^3}{9\pi}+\frac{m_a^2}{6}}\end{aligned} \tag{14}$$

In the same way, the ripple current through the filter inductor of grid-connected single-phase half-bridge inverters consists of triangle waves bounded by $\Delta i_{pp}/2$, as described by Fig.9.

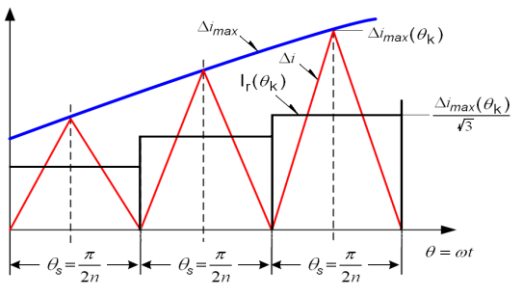

Fig. 8. RMS calculation of the equivalent filter inductor ripple current $\triangle i$.

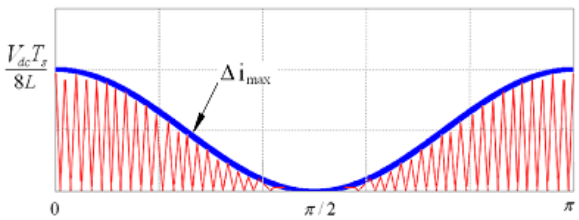

Fig. 9. Equivalent RMS waveform of filter inductor ripple current $\triangle i$ of single-phase half-bridge inverters.

Thus, the RMS value of the switching ripple current in single-phase half-bridge inverters can be calculated by (15)

$$\begin{aligned}I_r&=\frac{V_{dc}T_s}{8L}\sqrt{\frac{2}{3\pi}\frac{\pi}{2}\left(1-m_a^2+\frac{3}{8}m_a^4\right)}\\&=\frac{V_{dc}T_s}{8L}\sqrt{\frac{m_a^4}{8}-\frac{m_a^2}{3}+\frac{1}{3}}\end{aligned} \tag{15}$$

3. Filter Design Guideline

3.1 Filter design on full-bridge topology

The fundamental component for the filter inductor current of grid-connected single-phase full-bridge inverters can be calculated with (16).

$$I_1=\frac{m_aV_{dc}}{\sqrt{2}Z_{base}}=\frac{m_aV_{dc}}{2\sqrt{2}\pi f_oL_b}, \tag{16}$$

where f_o: utility frequency.

Thus, the switching ripple factor of grid-connected single-phase full-bridge inverters (RF_{sw}) is calculated by (17).

$$RF_{sw} = \frac{I_r}{I_1} = \frac{f_o}{f_{sw}} \cdot \frac{L_b}{L} \cdot \sqrt{\frac{\pi^2}{16} m_a^2 - \frac{4\pi}{9} m_a + \frac{\pi^2}{12}}, \quad (17)$$

where f_{sw}: inverter switching frequency (=$1/T_s$).

Conversely, when the ripple factor of the injection current is given by RF_{sw}, the filter inductor must be determined using (18).

$$\frac{L}{L_b} \geq \frac{1}{RF_{sw}} \cdot \frac{f_o}{f_{sw}} \cdot \sqrt{\frac{\pi^2}{16} m_a^2 - \frac{4\pi}{9} m_a + \frac{\pi^2}{12}} \ [pu] \quad (18)$$

3.2 Filter design on half-bridge topology

The fundamental component for the filter inductor current of grid-connected single-phase half-bridge inverters can be calculated with (19).

$$I_1 = \frac{m_a V_{dc}}{2\sqrt{2} Z_{base}} = \frac{m_a V_{dc}}{4\sqrt{2}\pi f_o L_b} \quad (19)$$

Thus, the switching ripple factor of grid-connected single-phase half-bridge inverters (RF_{sw}) is calculated by (20).

$$RF_{sw} = \frac{f_o}{f_{sw}} \cdot \frac{L_b}{L} \cdot \frac{\pi}{m_a} \sqrt{\frac{m_a^4}{16} - \frac{m_a^2}{6} + \frac{1}{6}} \quad (20)$$

When the ripple factor of the injection current is given by RF_{sw}, the filter inductor must be determined using (21).

$$\frac{L}{L_b} \geq \frac{1}{RF_{sw}} \cdot \frac{f_o}{f_{sw}} \cdot \frac{\pi}{m_a} \cdot \sqrt{\frac{m_a^4}{16} - \frac{m_a^2}{6} + \frac{1}{6}} \ [pu] \quad (21)$$

3.3 Filter design example

Table 1 describes circuit conditions for an example grid-connected PV inverter.

Table 1. Circuit conditions for grid-connected inverters.

Item	Condition
Rated Power P	10kVA
Rated Voltage V	220V
Utility frequency f_o	60Hz
Switching frequency f_{sw}	6kHz

The per-unit system for the circuit condition can be calculated as follows:

$$I_b = \frac{P}{V} = 45.45[A] \quad (22)$$

$$Z_b = \frac{V^2}{P} = 4.84[\Omega] \quad (23)$$

$$L_b = \frac{Z_b}{2\pi f} = 12.84[mH] \quad (24)$$

For example, to get the switching ripple factor under 10%, the filter inductance for a single-phase PV inverter can be designed using Table 2 and Table 3. Table 2 is for full-bridge inverters, and Table 3 is for half-bridge inverters. Per-unit filter inductance data in Table 2 and Table 3 can be applied to any power rating and any voltage rating. When the modulation index is m_a=1.0, the filter inductance of a single-phase half-bridge inverter is around 3.79 times that of a single-phase full-bridge inverter. When the modulation index is m_a=0.8, the filter inductance of a single-phase half-bridge inverter is around 3.63 times that of a single-phase full-bridge inverter.

Table 2. Filter inductance for single-phase full-bridge inverters.

Modulation Index	Filter inductance	
	Per-unit [pu]	Real [mH]
m_a=1.0	0.02075	0.266
m_a=0.8	0.03166	0.406

Table 3. Filter inductance for single-phase half-bridge inverters.

Modulation Index	Filter inductance	
	Per-unit [pu]	Real [mH]
m_a=1.0	0.07854	1.008
m_a=0.8	0.11489	1.475

To verify the relation between the switching ripple factor and the filter inductance on utility-interactive single-phase full-bridge inverters, simulation is done by PSIM.

Fig. 10 shows the simulation model for a utility-interactive single-phase full-bridge inverter by PSIM. Fig. 11 is the simulation model for a utility-interactive single-phase half-bridge inverter.

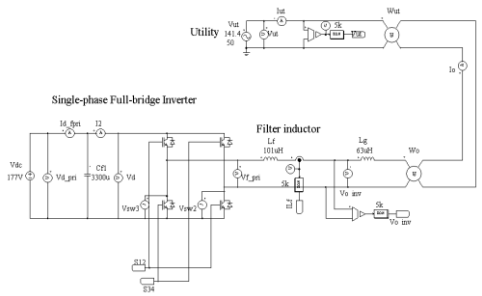

Fig. 10. Simulation model of utility-interactive single-phase full-bridge inverter.

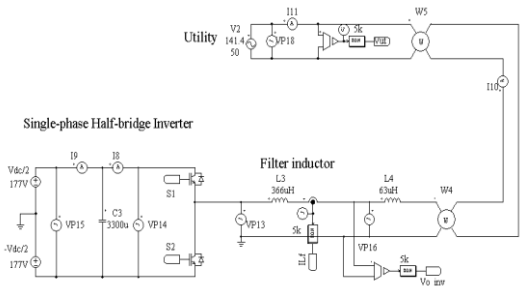

Fig. 11. Simulation model of utility-interactive single-phase half-bridge inverter.

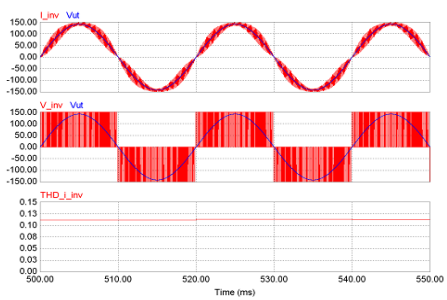

Fig. 12. Simulation waveform of utility-interactive single-phase. full-bridge inverter when m_a=1.0.

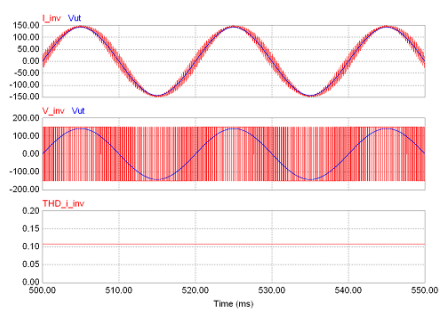

Fig. 13. Simulation waveform of utility-interactive single-phase half-bridge inverter when m_a=1.0.

Fig. 12 shows the simulation results for the single-phase full-bridge inverter when the modulation index is m_a=1.0. As expected by the analysis, the magnitude of the ripple component varies by a quadruple factor during the utility cycle. The ripple factor RF_{sw} is around 10% as expected by the proposed theory.

Fig. 13 shows the simulation results for the single-phase half-bridge inverter when the modulation index is m_a=1.0. As expected by the analysis, the magnitude of the ripple component varies twice during the utility cycle. The ripple factor RF_{sw} is around 10% as expected by the proposed theory.

4. Experimental Verification

To verify the presented theory regarding the switching ripple factor and the filter inductance of grid-connected single-phase inverters, experiments were conducted using a 10kVA/ 220V grid-connected PV inverter as described in Fig. 14.

The experimental conditions are listed in Table 1. The modulation index was set to m_a=0.8 throughout the experiment.

The experimental verification goes opposite way to the simulation process demonstrated before. Since precise implementation of a filter inductor is not easy, an available filter inductor was first selected in the laboratory, then the switching ripple factor $RF_{sw,mes}$ was measured using the selected filter inductor. Next, the switching ripple factor $RF_{sw,est}$ was estimated using (17) or (20) by applying the same filter inductances used in the experiment. Then, the measured ripple factor $RF_{sw,mes}$ and the estimated ripple factor $RF_{sw,est}$ were compared to verify the proposed theory.

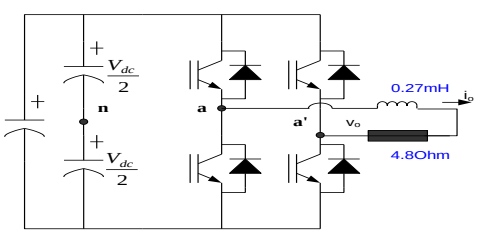

Fig. 14. Experimental set of grid-connected single-phase full-bridge inverter.

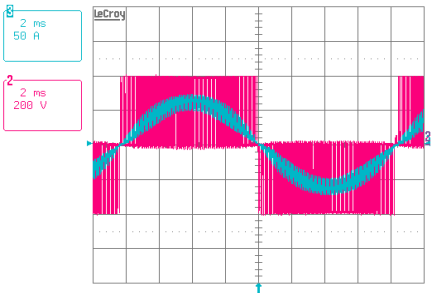

Fig. 15. Experimental waveform of grid-connected single-phase full-bridge inverters when m_a=0.8.

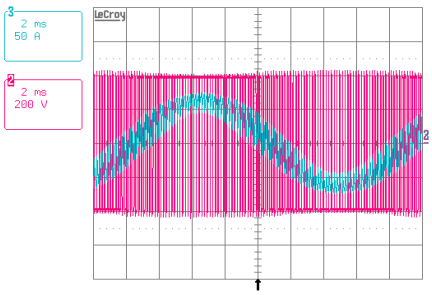

Fig. 16. Experimental waveform of grid-connected single-phase half-bridge inverters when m_a=0.8.

Table 4 demonstrates the experimental results from the proposed filter design guideline for a grid-connected single-phase full-bridge inverter and a half-bridge inverter, respectively. The half-bridge inverter was implemented by adopting bipolar PWM topology to the same experimental system.

Table 4. Experimental results for proposed grid-connected single-phase inverters.

PWM topology	Filter Inductor [mH]/[pu]	Ripple Factor	
		$RF_{sw,est}$ [%]	$RF_{sw,mes}$ [%]
Unipolar	0.27/0.021	15.0766	14.5
Bipolar	0.505/0.039	29.2351	28.4

Fig. 15 shows the experimental waveforms of the grid-connected single-phase full-bridge inverter with a filter inductance of 0.27 [mH] whose per-unit value is 0.021 [pu]. As expected by the theory, the magnitude of the ripple component varies as much as four times during the utility cycle.

Applying the equivalent per-unit filter inductance, Equation (17) estimates the switching ripple factor of the inductor current in the single-phase full-bridge inverter as $RF_{sw,est}$ =15.0766 [%]. From fast Fourier transform (FFT) analysis for the measured filter inductor current, the switching ripple factor $RF_{sw,mes}$ can be calculated to around 14.5 [%] of the rated RMS current. This is 96.17 [%] against the estimated switching ripple factor $RF_{sw,est}$. Thus the error is about -4 [%].

Fig. 16 shows the experimental waveforms of the grid-connected single-phase half-bridge inverter with a filter inductance of 0.505 [mH] whose per-unit value is 0.0393 [pu]. As expected by the theory, the magnitude of the ripple component varies twice during the utility cycle.

Applying the equivalent per-unit filter inductance, equation (20) estimates the switching ripple factor of the inductor current in the single-phase half-bridge inverter as $RF_{sw,est}$ =29.2351 [%]. From FFT analysis of the measured filter inductor current, the switching ripple factor $RF_{sw,mes}$ can be calculated to around 28.4 [%] of the rated RMS current. This is 96.17 [%] against the estimated switching ripple factor $RF_{sw,est}$. Thus, the error is about -3 [%].

However, the error is expected to decrease further if the experimental system uses a rated load resistor of 4.84 [Ω] instead of the 4.80 [Ω] load resistor currently used, which is 99 [%] to the rated resistance.

5. Conclusion

This paper has proposed and experimentally verified design guidelines for the filter inductor of grid-connected single-phase inverters. The RMS values of the fundamental component and ripple component for the filter inductor current of grid-connected single-phase inverters were analyzed qualitatively and quantitatively. Based on the ripple current analysis, design guidelines for filter inductors against the limitation of ripple factor were presented. Experimental results verified that the proposed filter design guidelines are very precise with the error under 4 [%]. The proposed design guideline is useful not only to achieve accurate filter inductance in *L*-filter design, but also to get necessary intermediate filter inductance in *LCL*-filter design. The proposed RMS calculation of the switching ripple current can be used for loss calculation of grid-connected single-phase inverter systems.

Acknowledgment

This work was supported by a research grant from Kongju National University in 2009.

This work was supported by Korea Research Foundation Grant funded by the Korean Government (KRF-D00162).

References

[1] F.Blaabjerg, Z.Chen, "Power Electronics as an Enabling Technology for Renewable Energy Integration," *Journal of Power Electronics*, Vol.3, No.2, pp. 81-89, 2003.

[2] Yaosuo Xue, Liuchen Chang, Sren Baekhj Kjaer, J. Bordonau, T. Shimizu, "Topologies of single-phase inverters for small distributed power generators: an overview," *IEEE Transactions on Power Electronics*, Vol. 19, pp 1305–1314, Sept. 2004.

[3] Qingrong Zeng; Liuchen Chang; "Study of advanced current control strategies for three-phase grid-connected pwm inverters for distributed generation," *in Proc. of 2005 IEEE Conference on Control Applications*, pp.1311–1316, Aug. 2005.

[4] Zhilei Yao, Zan Wang, Lan Xiao, Yangguang Yan, "A novel control strategy for grid-interactive inverter in grid-connected and stand-alone modes," *Applied Power Electronics Conference and Exposition.*, pp.779-783, March. 2006.

[5] Li Peng, Yong Kang, Xuejun Pei, Jian Chen, "A Novel PWM Technique in Digital Control," *Trans. on Industrial Electronics*, Vol. 54, No. 1, pp. 338-346, 2007.

[6] Abdul Rahiman Beig, G. Narayanan, V. T. Ranganathan, "Modified SVPWM Algorithm for Three Level VSI With Synchronized and Symmetrical Waveforms," *Trans. on Industrial Electronics*, Vol. 54, No. 1, pp. 486-494, 2007.

[7] Gan Dong, O. Ojo, "Current Regulation in Four-Leg Voltage-Source Converters," *Trans. on Industrial Electronics*, Vol. 54, No. 4, pp. 2095-2105, 2007.

[8] IEEE Standard P1547 Std: Standard for Interconnecting Distributed Resources with Electric Power Systems.

[9] Twining and D. G. Holmes, "Grid current regulation of a three-phase voltage source inverter with an LCL input filter," *IEEE Transactions on Power Electronics.*, Vol. 18, pp.888-895, May 2003.

[10] M. Prodanovic and T. C. Green, "Control and filter design of three-phase inverters for high power quality grid connection", *IEEE Transactions on Power Electronics*., Vol. 18, pp. 373-380, Jan. 2003.

[11] M.Liserre, F.Blaabjerg, S.Hansen, "Design and control of an *LCL*-filter based three-phase active rectifier*," IEEE Trans. on Ind. App*., Vol.38, No.2, pp.299-307, 2001.

[12] T.CY.Wang, Z.Ye, G.Sinha, X.Yuan, "Output Filter Design for a Grid-interconnected Three-Phase Inverter," *in Conf. Rec. on PESC'03*, Vol.2, pp.779-784, June 2003.

[13] Xiyou Chen, Dianguo Xu, Fengchun Liu, Jianqiu Zhang, "A Novel Inverter-Output Passive Filter for Reducing Both Differential- and Common-Mode dv/dt at the Motor Terminals in PWM Drive Systems," *Trans. on Industrial Electronics*, Vol. 54, No. 1, pp. 419-426, 2007.

[14] Jae-Seok Noh, Jaeho Choi, "Design of Voltage Source PWM Converter with AC Input *LCL* Filter," *Journal of Power Electronics*, Vol. 7, No. 5, pp.490-498, 2002.(Korean)

[15] T. Shimizu, T. Fujita, G Kimura, J. Hirose, "A unity power factor PWM rectifier with DC ripple compensation," *Trans. on Industrial Electronics*, Vol. 44, No. 4, pp. 447-455, 1997.

[16] F.M.P. Hidalgo, J.R.H. Larmbia, J.L.D. Pat, "Ripple reduction in DC line of a PWM drive by direct reinjection," *Trans. on Industrial Electronics*, Vol. 47, No. 4, pp. 971-973, 2000.

[17] F. Forest, E. Labourý, T. A. Meynard, V. A. Smet, "Design and Comparison of Inductors and Inter cell Transformers for Filtering of PWM Inverter Output," *IEEE Transactions on Power Electronics*, Vol. 24, No.3, pp.812-821, 2009.

Hyosung Kim (S'90-M'96) received B.S. and M.S. degrees in Electrical Engineering from Seoul National University in Korea on 1981 and 1983, respectively, and received the Ph.D. degree from Chungbuk National University on 1995. From 1982 to 1986, he was employed at Tong-Yang Cement Mfg. Co., Korea, where he participated in the factory automation and energy saving project. From 1996 to 1997, he was a visiting scholar in the Dept. of Electrical Engineering at Okayama University, Japan. From 2000 to 2001, he was an associate research professor in the Institute of Energy Technology at Aalborg University, Denmark. From 1997 to present, he is a tenured professor in the school of Electrical and Electronics Engineering at Kongju National University, Korea. He is interested in Power Quality, Static Compensators, Renewable energy, and Line interactive inverters.